

PIV Study on the Interaction of Triple Transitional Round Fountains in a Homogeneous Fluid

H. Mahmud¹, B. Hill¹, W. Gao², W. Lin^{1,2}, Y. He¹ and S. W. Armfield³

¹School of Engineering and Physical Sciences
 James Cook University, Townsville, QLD 4811, Australia

²Solar Energy Research Institute
 Yunnan Normal University, Kunming, Yunnan 650092, P. R. China

³School of Aerospace, Mechanical and Mechatronic Engineering
 The University of Sydney, NSW 2006, Australia

Abstract

This paper investigates experimentally the transient behavior of the interaction of triple transitional fountains injected from three round sources into a homogeneous fluid using the PIV technique over the Reynolds and Froude numbers in the ranges $100 \leq Re \leq 1000$ and $1 \leq Fr \leq 10$. The results show that the behavior of the interaction can be categorized into several distinct regimes: (a) Flapping steady regime, where the flow in the interaction region sways horizontally initially but soon becomes stable with no fluctuation in the interaction height and negligible horizontal sway; (b) Bobbing-flapping steady regime, where the interaction region bobs initially with a repeated up-and-down height and three-dimensional horizontal swaying behaviour, but at full development, the interaction becomes steady; (c) Flapping unsteady and bobbing-flapping unsteady regimes, where the behaviours of steady and unsteady interactions are quite similar with the exception that, in the unsteady regime, the interaction remains unsteady even at full development, with fluctuating maximum interaction height and continual swaying; and (d) Transitional/turbulent unsteady regime, where the interaction demonstrates strong unsteadiness and oscillating behavior starting from the beginning. All these observed characteristics are also mapped into a Re - Fr diagram.

Introduction

Negatively buoyant jets, commonly called fountains, are very common phenomenon in industry, geophysics and environments. Whenever any denser fluid is steadily injected upwards into a less dense fluid or in the opposite case when any lighter fluid is injected downward into a denser fluid a fountain like flow structure forms. The fountain flow behavior can be fully characterized by the dimensionless parameters the Reynolds number Re and the densimetric Froude number Fr , which are defined as follows,

$$Re = \frac{V_0 R_0}{\nu}, \quad Fr = \frac{V_0}{[R_0 g']^{1/2}}, \quad (1)$$

where V_0 is the mean inlet velocity of the jet fluid at the source, R_0 is the radius of the source, ν is the kinematic viscosity of fluid, $g' = g(\rho_0 - \rho_a)/\rho_a$ is the reduced gravity between the fluid at the source and the ambient fluid, g is the acceleration due to gravity, ρ_0 and ρ_a are the densities of the jet fluid and the ambient fluid at the source, respectively.

There are numerous situations where fountain type structure arises, such as the heating, ventilation and air conditioning of a large building structure, forced cooling of turbines, replenishment of magma chambers in the earth crust, disposal and management of brines, municipality sewerage and industrial waste into ocean, water quality management in reservoir or small lakes, evolution of volcanoes, replenishing of cold salt water at the bottom of a solar pond.

Kaye and Hunt [2] classified a round fountain as either “very weak” ($0 < Fr < 1$), “weak” ($1 < Fr < 3$), or “forced” ($Fr > 3$). The major features of forced fountain flows include the buoyancy forces are weak compared with the source momentum flux (thus also called “strong” fountains); the inner upflow of the fountain fluid behaves like a turbulent jet with strong mixing and entrainment of the ambient fluid (thus also called “turbulent” fountains) while the outer downflow of the fountain fluid behaves more like a dense plume; both the upflow and downflow continue to develop along their trajectories so the flow never attains self-similarity and the flow statistics vary with the axial location and the Froude number; and the fountain penetrates a large distance into the ambient fluid. On the other hand, in very weak or weak fountains, the discharge momentum flux of a fountain flow plays a less important role than the negative buoyancy flux and the flow is in the laminar or transitional regime (thus also called “laminar” or “transitional” fountains). For these weak fountains, it has been shown that their flow behavior is considerably different from that of forced fountains [1, 2, 3, 10]. For example, it has been shown that Z_m is smaller than R_0 for weak fountains while for forced fountains Z_m is much larger than R_0 , where Z_m is the maximum fountain penetration height; there are no distinguishable upward and downward flows in weak fountains, instead, the streamlines curve and spread from the fountain sources, while in forced fountains, the upward and downward flows are clearly distinguished; there is usually little entrainment of the ambient fluid into the fountain fluid in weak fountains while such an entrainment is one of the major activities occurring in forced fountains; the Reynolds number affects the penetration height in laminar fountains whereas in forced fountains it does not.

So far the studies on fountains have focused on fountains injected from a single source, in particular the single forced fountains. The most common parameter used in characterizing these fountain flow behaviour is Z_m , which is normally made dimensionless as $z_m = Z_m/R_0$. For a single forced fountain ejected from a round source into a homogeneous fluid, it has been found that $z_m = CFr$, where C is a constant of proportionality. $C = 2.46$ was found by many studies [1, 2, 9], although other values of C have also been reported. The readers are referred to some recent studies, such as Williamson et al. [10] and Burridge and Hunt [1] for the details.

For laminar and transitional round fountains the consensus seems to be that in addition to the momentum flux and buoyancy flux the fluid viscosity also plays an important role [2, 4, 10], leading to the conclusion that z_m is also under the influence of Re and several scalings have been developed. For example, Lin and Armfield [4] showed that for transitional round fountains dimensional consistency requires $z_m = C_1 Fr Re^n$, where n is a constant which is found to be dependent on Fr and Re and C_1 is a constant of proportionality. However, a wide range of n values

have been obtained for different values of Fr and Re , again as summarized by Williamson et al. [10] and Burrige and Hunt [1].

The onset of instability and unsteadiness in fountains is the key to elucidate the mechanism for the generation of turbulence and entrainment in fountains but is not well understood, although some attempts have been made recently, such as that by [5] and [10].

The interaction of multiple source jets/plumes is very common and important phenomenon in many applications such as cooling and heating in food industry, computers and electronic instruments, flow rising from industrial and households smokestacks, displacement ventilation and air conditioning of large building spaces. Despite these numerous application, this is an area that the studies are scarce and lacking [6, 7, 8]. To the authors best knowledge, no study has been found to investigate the interaction among multiple fountains, which motivate us to conduct this study to examine the behavior of interaction of triple transitional fountains by using flow visualization and non-invasive PIV technique.

Experimental Apparatus and Setup

Experiments have been conducted over the ranges of $100 \leq Re \leq 1000$ and $1 \leq Fr \leq 10$ by using a High-Framing-Rate Stereo PIV (HFR-SPIV) system, from Dantec Dynamics. In these experiments, triple round fountains were produced by injecting, through three identical round orifices, saline water vertically upwards into fresh water contained in a 24 cm diameter and 0.5 m height cylindrical Perspex-sided test tank as depicted in figure 1, where the experimental setup is depicted.

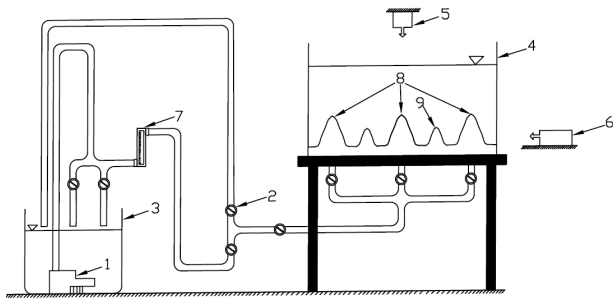


Figure 1: Schematic of the experimental setup: (1) saline water supply pump; (2) ball valve; (3) salt water tank; (4) fresh water tank; (5) double pulsed Nd-Yag laser source; (6) high resolution CCD camera; (7) flow meter equipped with needle valve; (8) triple fountains; (9) interactions.

Prior to the commencement of each experiment, the salt water tank was filled with fresh water. High quality salt and almost neutrally buoyant Nylon 12 Polyamide polymer spherical tracer particles (density 1030 kg/m^3 , mean diameter $50 \mu\text{m}$) were added into the salt water tank and well mixed using a Davey D15A submersible sump pump to achieve the desired uniform density of the saline water for the specific Froude number of the experiment. The Perspex-sided test tank was filled with fresh water from the mains up to the desired height, and Nylon 12 Polyamide polymer spherical tracer particles were also added and well mixed. After the saline water in the saline water tank and the fresh water in the test tank became stationary, their individual densities were measured by a hand-held Mettler Toledo Densito 30PX density meter which had an accuracy of 0.001 g/cm^3 .

A fountain flow was initiated by opening the ball valve to eject

saline water into the test tank at a fixed flow rate for the specific Reynolds number using the sump pump, and this flow was maintained in the course of the experiment. The volumetric flow rate was measured and controlled by an Aalborg high precision needle valve flow meter. In order to avoid clogging of seeded particles inside the flow meter, a water filter was installed before the entry section of the meter. The volumetric rates were maintained between 0.0451 l/min to 0.451 l/min . The density ratio $(\rho_0 - \rho_a)/\rho_a$ (ρ_0 for saline water and ρ_a for fresh water, both at the fountain sources) was varied between 0.00059763 and 0.05976289 .

The FlowManager of the Dantec PIV device controls the duration of the PIV experiment, the image capturing of the high speed camera (a Redlake HG-100K camera with a maximum resolution of 1504×1128 pixels and at a high framing rate of 30 fps), and the operation of the double pulsed laser (a Lee LDP-100MQG Nd: YAG laser emitting $0.532 \mu\text{m}$ radiations). The saline water inlet pipe was aligned flush with the floor of the fresh water tank and the saline water pipe was kept long enough to ensure that the flow entering the test tank was fully developed. A small amount of food dye was used for visualizing fountain flows.

Experimental ranges of Fr and Re are varied by adjusting salinity of saline water and inlet flow rate for a constant inlet nozzle size $R_0 = 2.5 \text{ mm}$. One jet source is placed at the centre of the test tank and the two other sources are located on the left and right side of the central fountain. The centre-to-centre distance between the central and the adjacent fountains is 10 mm , which is kept fixed for all of the conducted experiments.

Experimental Results and Discussion

The observed behavior of the interaction of triple fountains obtained from the current experiments can be categorized broadly into a steady and an unsteady regime. A demarcation line can be found to distinguish these two regimes. However, the exact location of the line cannot be determined in this study due to the restrictions on the experiments. Nevertheless, the experimental results show that the regime with $Re \leq 100$ and $Fr \leq 5$ and $100 \leq Re \leq 300$ at $Fr = 1$ can be roughly considered as in the steady regime and the remaining are in the unsteady regime, as summarized in the $Re - Fr$ regime mapping plot shown in figure 2, where a part of the results shown were obtained from another ongoing study on the interactions of triple round fountains by direct numerical simulation (DNS).

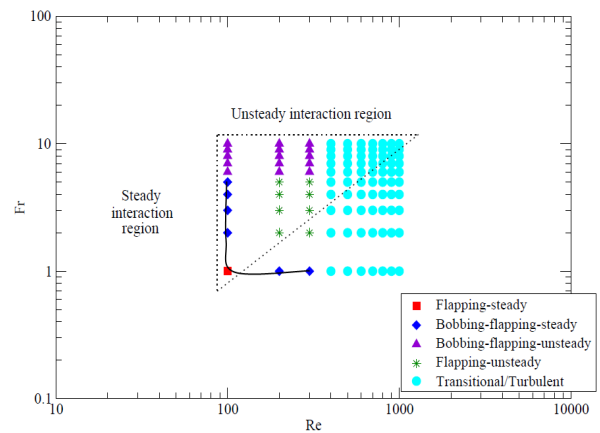


Figure 2: $Re - Fr$ regime map for the interactions of triple round fountains, where experimental results are located within dotted area and other results are from DNS.

From the experimental results, it is found that the steady regime can be further divided into two sub-regimes: flapping and bobbing-flapping. Due to insufficient experimental data, the exact ranges of Re and Fr for the flapping steady interaction cannot be determined. Among all experimental cases, only one case, that is, when $Re = 100$ and $Fr = 1$, the interaction is in the flapping steady regime. However, it is speculated that the interaction of some other triple round fountains with smaller Fr and Re values should also be in this sub-regime. In this sub-regime, the initial flow in the interaction region between two adjacent fountains sways horizontally around the middle plane of these two fountain sources with gradually increasing maximum interaction height for a very short period of time and then becomes stable with no fluctuation in the interaction height and negligible horizontal sways when the interactions attain full development. The evolution of a flapping steady interaction is captured in figure 3 for $Re = 100$ and $Fr = 1$. Figure 3(a-f) shows that the steady flapping interaction sways left and right and attains nearly maximum interaction height stages in figure 3(f). After that, it gradually comes to steady state without any fluctuation in height. It is also observed from the PIV images that the time-averaged maximum interaction height in the flapping steady regime stay on the middle plane between the adjacent fountain sources at the steady state.

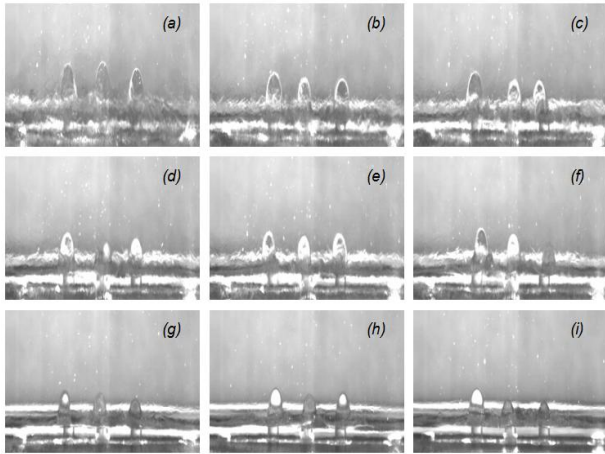


Figure 3: Typical PIV images showing the time evolution of the flapping steady interaction in triple round fountains with $Re = 100$ and $Fr = 1$ at (a) $\tau = 21.19$; (b) $\tau = 26.55$; (c) $\tau = 27.83$; (d) $\tau = 31.40$; (e) $\tau = 32.17$; (f) $\tau = 33.70$; (g) $\tau = 55.15$; (h) $\tau = 62.81$; and (i) $\tau = 81.7$, where τ is made dimensionless by R_0/V_0 .

The bobbing-flapping steady regime is observed for $2 \leq Fr \leq 5$ at $Re = 100$ and $200 \leq Re \leq 300$ at $Fr = 1$, as shown in figure 2. In this sub-regime, the peak of the interaction region initially moves upwards, comes to rest at a finite height and then collapses around the next rising peaks. This phenomenon repeats for a short period of time, demonstrating a bobbing behavior. At the same time, the interaction region sways horizontally, not limited on the plane passing through the fountain sources, showing a three-dimensional feature. After this, the interaction eventually becomes steady with no change of the maximum interaction height, which is located on the middle plane between the adjacent fountain sources, and again no further horizontal sway. The PIV images showing the time evolution of the bobbing-flapping steady interaction is shown in figure 4 for $Re=100$ and $Fr=3$. It is observed that the formation of interactions of fountains, the development of the penetration heights and the movement of interaction region are demonstrated in fig-

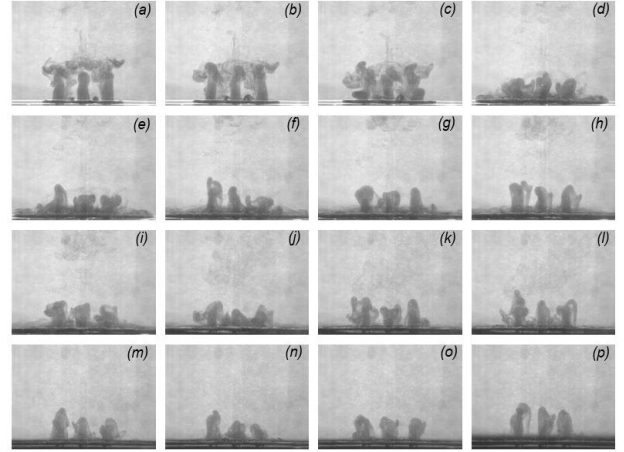


Figure 4: Typical PIV images showing the time evolution of the bobbing-flapping steady interaction in triple round fountains with $Re=100$ and $Fr=3$ at (a) $\tau = 20.42$; (b) $\tau = 21.70$; (c) $\tau = 22.97$; (d) $\tau = 29.36$; (e) $\tau = 30.63$; (f) $\tau = 32.93$; (g) $\tau = 35.74$; (h) $\tau = 40.85$; (i) $\tau = 43.40$; (j) $\tau = 53.61$; (k) $\tau = 61.27$; (l) $\tau = 63.83$; (m) $\tau = 99.57$; (n) $\tau = 114.89$; (o) $\tau = 120.00$; and (p) $\tau = 243.83$.

ure 4(a-n). After that, the interaction becomes stable with negligible change of its height for a long period of time, as shown in figure 4(o-p). It is also observed from the PIV images that the time-averaged maximum interaction height in the bobbing-flapping steady regime stay on the middle plane between the adjacent fountain sources at the steady state.

The unsteady interaction regime can be divided into three sub-regimes: flapping, bobbing-flapping and transitional/turbulent. The unsteady flapping regime is observed for $200 \leq Re \leq 300$ with $2 \leq Fr \leq 5$; the unsteady bobbing-flapping regime is in the ranges of $100 \leq Re \leq 300$ with $6 \leq Fr \leq 10$; and the unsteady transitional/turbulent regime is found for $400 \leq Re \leq 1000$ with $1 \leq Fr \leq 10$, as shown in figure 2.

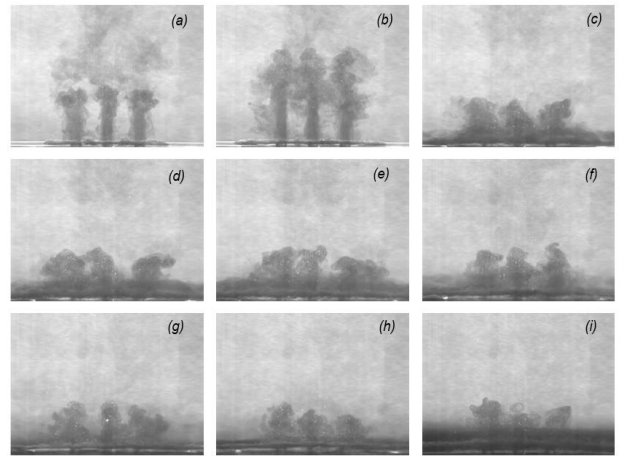


Figure 5: Typical PIV images showing the time evolution of the flapping-unsteady interaction in triple round fountains with $Re=300$ and $Fr=4$ at (a) $\tau = 38.30$; (b) $\tau = 45.96$; (c) $\tau = 61.28$; (d) $\tau = 65.11$; (e) $\tau = 68.94$; (f) $\tau = 91.92$; (g) $\tau = 130.22$; (h) $\tau = 160.87$; and (i) $\tau = 329.40$.

The flapping and bobbing-flapping unsteady interactions are quite similar with the exception that in the unsteady case the in-

interaction remains unsteady even at full development, with fluctuating maximum interaction height and continual sway.

The unsteady flapping interaction is presented in figure 5 for $Re=300$ and $Fr=4$, where the formation of unsteady interaction and the flapping behavior are clearly seen. The time average maximum interaction height in the flapping unsteady regimes stay away from the middle plane between the adjacent fountain sources as shown in figure 5(b).

Figure 6 presents the typical PIV images showing the time evolution of the bobbing-flapping-unsteady interaction with $Re = 200$ and $Fr = 7$. It exhibits the formation of unsteady bobbing-flapping interaction. After the initiation of interaction, initially its front rises up to a certain height, comes to rest, collapses around the next rising peaks and sways from one side to another side continuously while its height is always changing at full development of interaction.

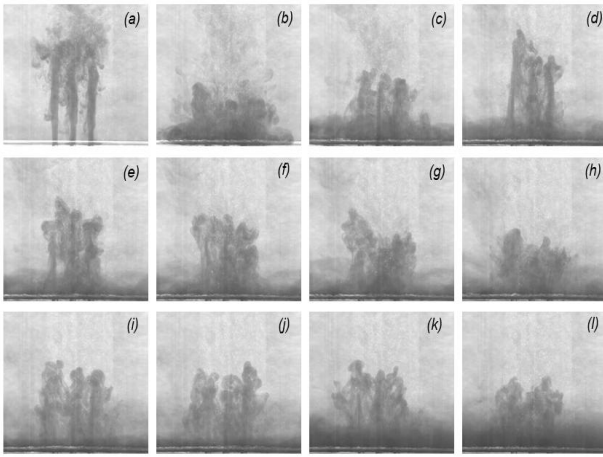


Figure 6: Typical PIV images showing the time evolution of the bobbing-flapping-unsteady interaction in triple round fountains with $Re=200$ and $Fr=7$ at (a) $\tau = 51.06$; (b) $\tau = 86.81$; (c) $\tau = 102.13$; (d) $\tau = 122.55$; (e) $\tau = 132.77$; (f) $\tau = 137.87$; (g) $\tau = 142.98$; (h) $\tau = 158.30$; (i) $\tau = 194.04$; (j) $\tau = 199.15$; (k) $\tau = 291.07$; and (l) $\tau = 342.13$.

Strong unsteadiness and oscillating behavior observes at the initial stage of an unsteady transitional/turbulent interaction which increases even after full development of interaction as shown in figure 7, where typical PIV images of an unsteady transitional/turbulent interaction is shown for $Re=600$ and $Fr=8$. The mechanism of formation of interaction, its unsteadiness, undulation of height can be seen from figure 7(a-d). Moreover the interaction collapses, re-laminarizes and rises through the collapsed interaction fluid as shown in figure 7(e-h).

Conclusions

In this study, the behavior of interactions of triple transitional round fountains in a homogeneous fluid is studied experimentally using flow visualization and noninvasive PIV technique over the range of $100 \leq Re \leq 1000$ and $1 \leq Fr \leq 10$. The results show that the behavior of interactions of these triple round fountains can be categorized into several regimes: flapping steady, bobbing-flapping steady, flapping-unsteady, bobbing-flapping-unsteady, and transitional/turbulent. The salient features of these observed regimes are discussed and finally summarized onto a $Re-Fr$ regime mapping plot.

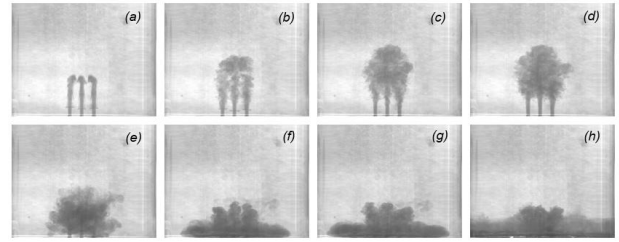


Figure 7: Typical PIV images showing the time evolution of the transitional/turbulent-unsteady interaction in triple round fountains with $Re = 600$ and $Fr = 8$ at (a) $\tau = 15.27$; (b) $\tau = 22.91$; (c) $\tau = 30.54$; (d) $\tau = 45.82$; (e) $\tau = 61.09$; (f) $\tau = 91.64$; (g) $\tau = 114.55$; and (h) $\tau = 183.29$.

Acknowledgements

The authors gratefully acknowledge the support of the National Natural Science Foundation of China (11072211, 50879074), the Natural Science Foundation of Yunnan Province (2011FA017), the Australian Research Council (ARC), the Specialized Research Fund for the Doctoral Program of Higher Education (20105303110001), and the Program for Changjiang Scholars and Innovative Research Team in University of Ministry of Education of China. The first author also acknowledges a James Cook University Postgraduate Scholarship.

References

- [1] Hunt, G. and Burrige, H., The Rise Heights of Low- and High-Froude-Number Turbulent Axisymmetric Fountains, *J. Fluid Mech.*, **691**, 2012, 392–416.
- [2] Kaye, N. and Hunt, G., Weak Fountains, *J. Fluid Mech.*, **558**, 2006, 319–328.
- [3] Lin, W. and Armfield, S., Direct Simulation of Weak Laminar Plane Fountains in a Homogeneous Fluid, *Int. J. Heat Mass Transfer*, **43**, 2000, 3013–3026.
- [4] Lin, W. and Armfield, S., The Reynolds and Prandtl Number Dependence of Weak Fountains, *Comput. Mech.*, **31**, 2003, 379–389.
- [5] Lin, W. and Armfield, S., Onset of Entrainment in Transitional Round Fountains, *Int. J. Heat Mass Transfer*, **51**, 2008, 5226–5237.
- [6] Linden, P. and Cooper, P., Natural Ventilation of an Enclosure Containing Two Buoyancy Sources, *J. Fluid Mech.*, **311**, 1996, 153–176.
- [7] Moses, E., Zocchi, G. and Libchaberii, A., An Experimental Study of Laminar Plumes, *J. Fluid Mech.*, **251**, 1993, 581–601.
- [8] Pera, L. and Gebhart, B., Laminar Plume Interactions, *J. Fluid Mech.*, **65**, 1975, 250–271.
- [9] Turner, J., Jets and Plumes with Negative or Reversing Buoyancy, *J. Fluid Mech.*, **26**, 1966, 779–792.
- [10] Williamson, N., Srinarayana, N., Armfield, S., McBain, G. and Lin, W., Low-Reynolds-Number Fountain Behaviour, *J. Fluid Mech.*, **608**, 2008, 297–318.